Conformational studies of a trisaccharide epitope in solution by using NMR spectroscopy and molecular mechanics and dynamics calculations with the MM3* program

Manuel Martín-Pastor, Juan Luis Asensio, Rosa López and Jesús Jiménez-Barbero *
Grupo de Carbohidratos, Dept. de Química Orgánica Biologica, Instituto de Química Orgánica, CSIC, Juan de la Cierva 3, 28006 Madrid, Spain

The solution conformations of methyl β-D-galactopyranosyl-(1→2)-xylopyranoside (**1**) and methyl α-L-fucopyranosyl-(1→2)-β-D-galactopyranosyl-(1→2)-xylopyranoside (**2**) have been analysed by NMR spectroscopy and molecular mechanics and dynamics calculations. The comparison between NMR experimental results (NOEs based on NOESY, ROESY, T-ROESY and steady-state experiments) and expected data [from ensemble average distributions of conformers and molecular dynamics (MD) simulations] indicates that both compounds present a moderate flexibility around their glycosidic linkages. A van der Waals interaction between the remote fucopyranosyl and xylopyranosyl moieties of **2** can be deduced from the theoretical and experimental data.

Recent studies have demonstrated that oligosaccharides are involved in a number of recognition events, *e.g.* cell adhesion, metastasis, fertilization and embryonic development.[1,2] Therefore, the understanding of how these molecules are recognized by the binding sites of lectins, antibodies and enzymes is currently a topic of major interest in bioorganic chemistry. To play a role in these functions, the three dimensional structure of the carbohydrate is of primary importance.[3,4] The extent and nature of the motion around the glycosidic linkages of oligosaccharides remains an open question,[5] and even detailed analysis of experimental and theoretical results have concluded either single rigid conformations[6] or conformational averaging[7] for different (or the same) carbohydrate structures. The existence of rigid or flexible structures is of prime importance in the recognition phenomenon, since any bimolecular binding process is, in principle, entropically unfavourable owing to the formation of a single molecular complex, which occurs with a decrease of rotational and translational entropy.[8] One of the most usual methods of establishing the solution conformation of biomolecules is the combination of NMR spectroscopy and molecular mechanics and dynamics simulations,[9] which is also currently being applied to the carbohydrate field.[10] Nevertheless, there are still important problems with the force field calculations that mainly arise from the lack of general valid parameter sets, which are usually insufficiently proven, and this is particularly true for oligosaccharide moieties. In this context, different force fields have been used in the conformational analysis of these molecules.[6,11-18] For instance, Homans has recently reported on the development and testing of a modification of the AMBER force field which has been parametrized to deal with saccharides.[19] On this basis, we now report on the conformational study of methyl β-D-galactopyranosyl-(1→2)-β-D-xylopyranoside (**1**) and methyl α-L-fucopyranosyl-(1→2)-β-D-galactopyranosyl-(1→2)-β-D-xylopyranoside (**2**) using NMR spectroscopy and MM3* molecular mechanics[20] and dynamics calculations, as a part of a project on the knowledge of the forces and structural motifs which mediate the molecular recognition of galactose-containing oligosaccharides by different lectins and enzymes.[21,22] In particular, trisaccharide **2**[23] is a fragment of a nonasaccharide repeating unit of plant cell xyloglucan, which acts as an endogenous hormone to regulate cell growth.[24] This trisaccharide is postulated to be the minimum structural feature responsible for the inhibition of 2,4-dichlorophenoxyacetic acid-stimulated growth of the pea stem.[25]

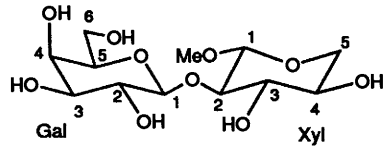

1

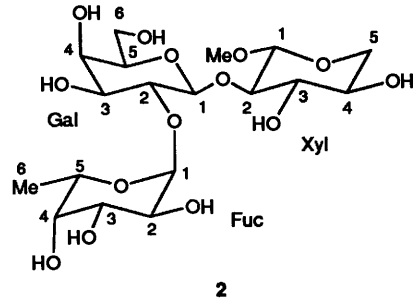

2

Results and discussion

A relaxed energy plot of the isoenergy contours obtained for β-D-Gal-(1→2)-β-D-Xyl-OMe (**1**) using the MM3* force field ($\varepsilon = 4$) is shown in Fig. 1(*a*). It is observed that there is a broad low energy region separating two smaller islands. Fig. 2 shows views of the main three low energy conformers of **1**. The previously reported experimental and theoretical structures for different β(1→2) equatorial-linked disaccharides[26,27] are included in the low energy region close to minimum A. Two additional minima (A1, A2) are located in this region. These minima have a small energy barrier between them and therefore are barely detectable. This low energy region is fairly extended, mainly around Ψ and is defined by Φ values between −60° and 80° and a set of Ψ values ranging between −70° and 70°, *i.e. ca.* 16% of the total area. The other two energy regions around conformers B and C are narrower and account for an additional 6% of the two dimensional energy surface. The energy barrier between minima A and B is *ca.* 6 kcal mol^{-1}.

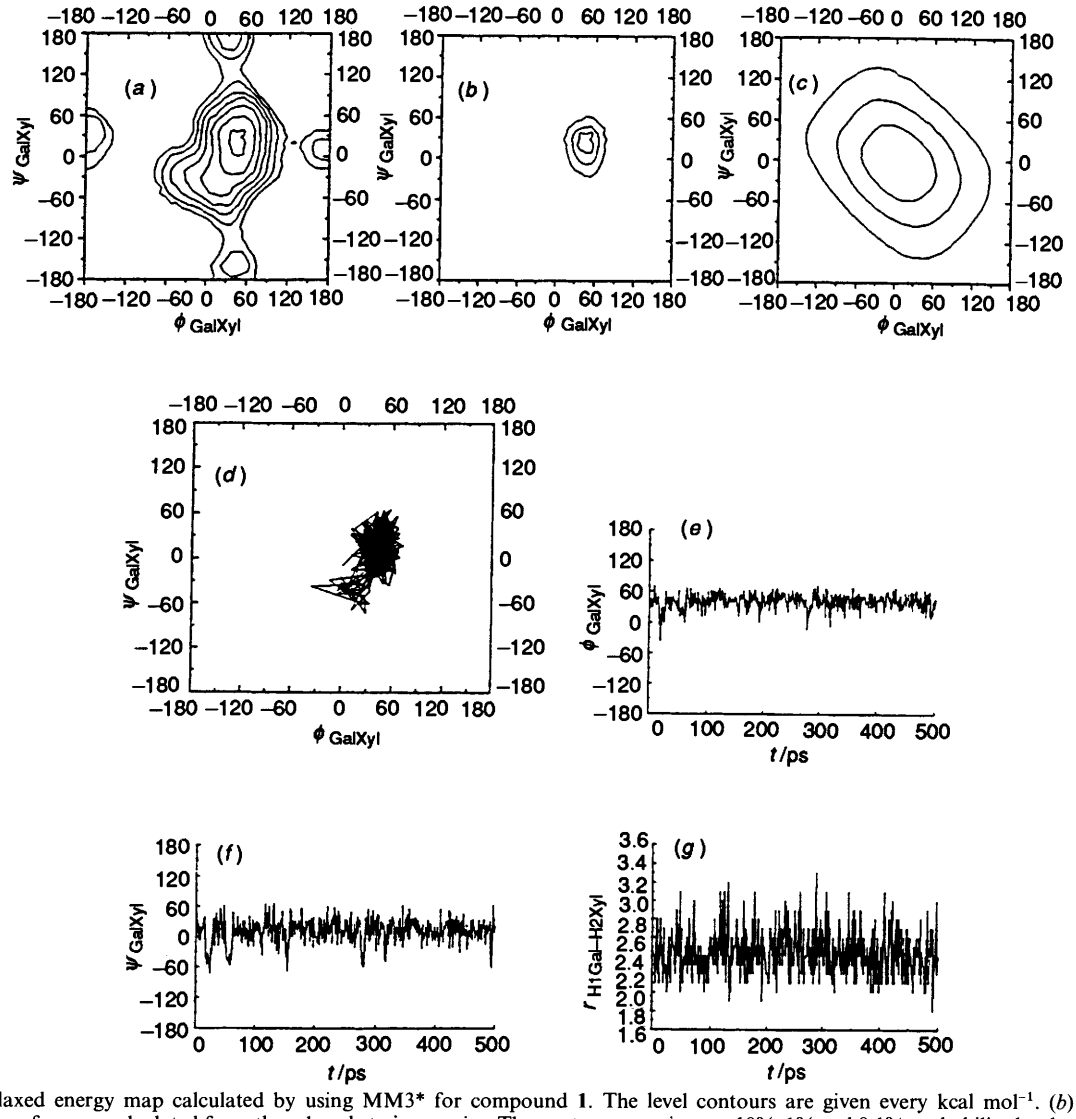

Fig. 1 (*a*) Relaxed energy map calculated by using MM3* for compound **1**. The level contours are given every kcal mol^{-1}. (*b*) Probability distribution of conformers calculated from the relaxed steric energies. The contours are given at 10%, 1% and 0.1% probability levels. (*c*) Relevant interproton distance of **1**: Gal-1-H–Xyl-2-H. The levels are drawn at 2.5, 3.0 and 3.5 Å. (*d*) Trajectory plots of one MD simulation for **1**, starting from minimum A. Trajectory of the simulation in Φ/Ψ space. (*e*) History of Φ. (*f*) History of Ψ. (*g*) History of the Gal-1-H–Xyl-2-H distance.

while that between B and C is *ca.* 5 kcal mol^{-1}. The single point populations, calculated from the steric energy differences, indicate that the population around minimum A is more than 98%, while the two minor islands described by minima B and C are populated by less than 1% each. The conformation minima A and C are as predicted by the *exo*-anomeric effect.[27]

In a first step, the exploration of the conformational space of trisaccharide α-L-Fuc-(1→2)-β-D-Gal-(1→2)-β-D-Xyl-OMe (**2**) through molecular mechanics calculations was limited to the energy regions allowed for the component disaccharide **1**. Thus, three different relaxed energy maps were calculated for **2** by rotating the glycosidic angles around the Fuc-Gal moiety using geometries which differed in the starting orientation of the Gal-Xyl fragment [from minima A, B and C]. In addition, the map for the isolated disaccharide entity, *i.e.* α-L-Fuc-(1→2)-β-D-Gal, was also calculated. These maps are remarkably similar and show a common broad low energy region (Fig. 3). Φ angles are positive and quite restricted towards *exo*-anomeric values (*ca.* 50°), while Ψ angles range between −80° and 80° (*ca.* 12% of the complete potential energy surface) and are independent of the starting conformation of the Gal-Xyl disaccharide fragment. In addition, it can be observed that there are also two smaller valleys, derived from the low energy region towards negative Φ angles (around Φ/Ψ, −50°/−40°) or towards $\Psi = 180°$, but their energies are too large to be further considered. These observations seem to indicate that, according to the MM3* calculations, the orientation of the xylose moiety does not significantly affect the conformational behaviour of the Gal-Fuc moiety. The global minima of each relaxed map is described by the following torsion angles. Min A′: $\Phi_{Fuc-Gal}$ 43°, $\Psi_{Fuc-Gal}$ 31°, $\Phi_{Gal-Xyl}$ 45°, $\Psi_{Gal-Xyl}$ 25°. Min B′: $\Phi_{Fuc-Gal}$ 42°, $\Psi_{Fuc-Gal}$ 32°, $\Phi_{Fuc-Xyl}$ 41°, $\Psi_{Gal-Xyl}$ 174°. Min C′: $\Phi_{Fuc-Gal}$ 31°, $\Psi_{Fuc-Gal}$ 37°, $\Phi_{Gal-Xyl}$ −168°, $\Psi_{Gal-Xyl}$ 58°. The single point population obtained for minimum A′ is more than 99.8%, although according to the shape of the relaxed maps, the presence of conformational mobility, mainly around angle Ψ, seems to be granted.

The conformational stability of **1** and **2** was studied through MD simulations. Thus, the geometries describing the global minima for both **1** and **2** were taken as starting structures for independent calculations. The MD trajectory of **1** is displayed in Fig. 1(*b*). It can be observed that the trajectory sampled the whole low energy region during the simulation, with no transitions to the small islands described by minima B and C. Besides, four independent simulations, using different conditions (MM3*, bulk relative permittivity ε = 1, 4 and 80, and

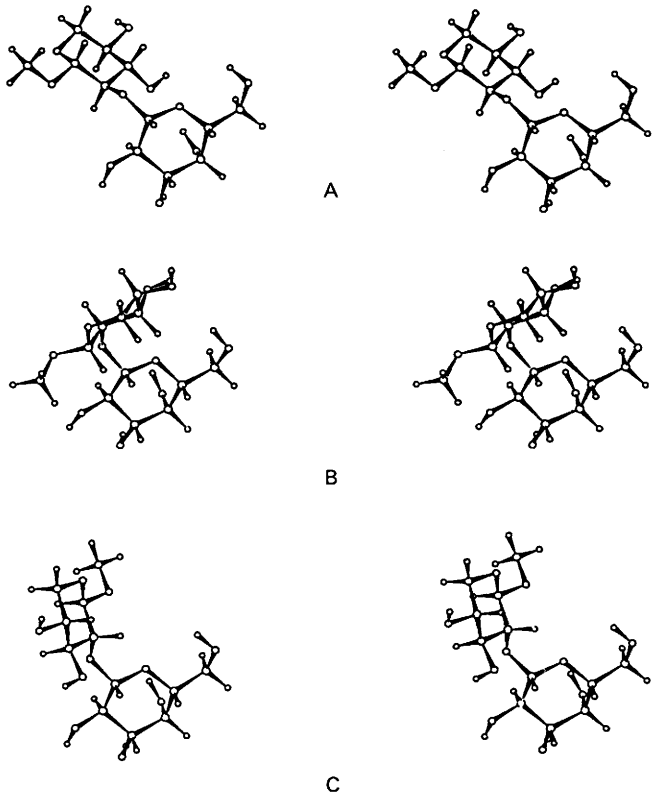

Fig. 2 Stereoscopic views of the MM3* low energy conformers of **1**

with solvent, according to the GB-SA model)[28] were carried out for **2**. In these cases, the trajectories remained within the low energy regions, too [Fig. 3(*b*)]. The relative permittivity basically has no influence on the result of the simulation. Therefore, and according to these calculations, the regions described by conformers A and A′, for **1** and **2**, respectively, are heavily populated. Fig. 4 shows a view of conformer A′. Conformers A and A′ do not show any inter-residue hydrogen bonding. However, from the inspection of the model, a van der Waals interaction can be deduced involving the C-5–C-6 region of the Fuc moiety and the α-face (3-H) of the Xyl unit. Note that conformer A′ is similar to the conformers reported using different force fields for other L-Fuc-(1→2)-β-D-Gal-containing oligosaccharides.[27,29–32] The difference between **2** and these other oligosaccharides resides is in the remote residues attached to the galactopyranosyl moiety. Thus, **2** has a 2-*O*-substituted methyl xylopyranoside, while the other oligosaccharides present 3-*O*-substituted GlcNAc, 3-*O*-substituted GalNAc or 4-*O*-substituted Glc(GlcNAc) rings.[6,27,29–31] Therefore, it is interesting to note that **2** is related to the blood group H oligosaccharides.[32] Since the nature and configuration of the groups which flank the glycosidic linkage in either case are rather different, their remote interactions with the fucopyranosyl moiety could drive the conformation of the Fuc-Gal linkage to different regions. In fact, the existence of equilibrium between conformers having negative and positive Φ angles has been reported for this fragment in several mono- and di-fucosyllactoses in DMSO solution.[33] Nevertheless, it seems that according to the calculations, there are no major changes in the conformation of the Fuc-Gal moiety.

With regard to the galactose hydroxymethyl group, several transitions between the *gt* and *tg* rotamers were observed for **2** when using MM3* at both relative permittivities while, for **1**, the trajectory stayed in the *gt* orientation for the whole simulation.

Table 1 ^{1}H and ^{13}C NMR chemical shifts (δ) for **1** and **2** in D_2O at 37 °C

	Xyl residue		Gal residue		Fuc residue	
	^{1}H	^{13}C	^{1}H	^{13}C	^{1}H	^{13}C
Compound **1**						
1-H	4.48	106.0	4.70	105.2		
2-H	3.58	82.4	3.55	71.9		
3-H	3.54	71.8	3.56	75.8		
4-H	3.62	71.8	3.92	71.6		
5-H_{ax}	3.35	67.5	3.62	75.2		
5-H_{eq}	3.98					
6′-H_a			3.74	63.9		
6′-H_b			3.80			
Compound **2**						
1-H	4.41	103.4	4.93	102.0	5.27	101.1
2-H	3.68	77.3	3.63	77.4	3.81	69.5
3-H	3.57	76.6	3.84	73.8	3.90	71.2
4-H	3.62	69.5	3.89	70.5	3.84	73.2
5-H_{ax}	3.31	66.1	3.64	75.2	4.42	68.3
5-H_{eq}	3.97	66.1				
6′-H_S			3.72	61.5	1.23	18.2
6′-H_R			3.81			

NMR results

The validity of this conformational analysis has been tested with relaxation measurements, *i.e.* nuclear Overhauser enhancements[34] and non-selective relaxation times.[35] The previous step for the analysis of the NOE data was the assignment of the different resonances through a combination of regular DQF-COSY,[36] TOCSY[37] and HSMQC[38] techniques. The chemical shifts for **1** and **2** are shown in Table 1. The observed couplings (data not shown) agree with $^4C_1$ chair conformations for the Xyl and Gal rings and the $^1C_4$ chair for the L-Fuc pyranoid ring. With regard to the conformation of the galactose lateral chain, Gal-H-6$_{proR}$ and -H-6$_{proS}$ were assigned as previously reported for similar derivatives.[39] The distribution of rotamers was calculated, following well established methodology,[40] from the vicinal proton–proton coupling constants, assuming a *gt*:*tg* equilibrium among the rotamers.[41] The observed couplings (7.5 and 5.5 Hz) agree with combinations of the *gt* and *tg* rotamers, contribution of the *gt* rotamer[42] accounting for > 65%.

The experimental nuclear Overhauser enhancements, obtained *via* steady-state measurements and through NOESY[43] and ROESY[44] experiments (Figs. 5 and 6) are collected in Tables 2–4. T-ROESY experiments,[45] which remove the spurious contribution of Hartmann–Hahn effects in spin-locked-type NOE experiments, were also performed. The comparison of regular 1D- or 2D-ROESY peaks with T-ROESY enhancements (Fig. 7) indicated that despite careful setting of the radio frequency (RF) carrier for ROESY, it was not possible to eliminate completely the formation of spurious peaks through coherence transfer.[46] On the other hand these were indeed negligible in T-ROESY. The 300 and 500 MHz non-selective relaxation times are shown in Table 5. The observed NOEs and T_1 relaxation parameters for **1** correspond to an average correlation time for the molecule ($\tau_c < 10^{-10}$ s), clearly within the extreme narrowing limit ($\omega\tau_c$ *ca.* 2×10^{-1}). Next, the experimental NOE values obtained after different conditions, either in the laboratory frame (NOESY, 1D-NOE) or in the rotating frame (ROESY) were compared with the expected parameters, obtained as described in the experimental part, for the corresponding probability distributions and the MD trajectories. Figs. 1 and 3 also show the representation of the relevant inter-residue proton–proton distances in terms of the glycosidic torsion angles and the probability distribution

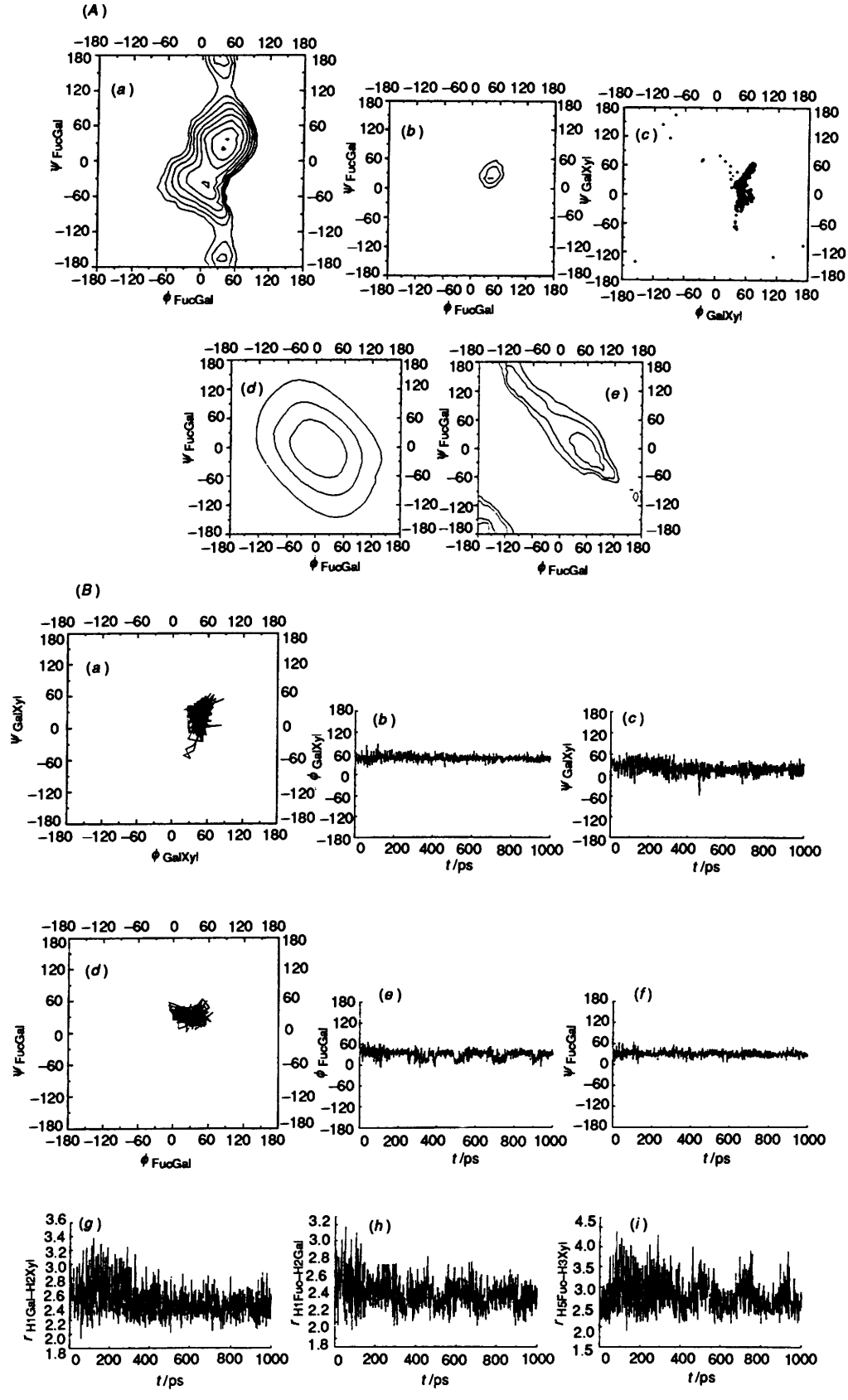

Fig. 3 (*A*) (*a*) Relaxed energy map calculated by using MM3* for compound **2**, starting from the global minimum for the Gal-Xyl disaccharide. The level contours are given every kcal mol^{-1}. (*b*) Probability distribution of conformers calculated from the relaxed steric energies. The contours are given at 10%, 1% and 0.1% probability levels. (*c*) Variation of the glycosidic torsion angles of Gal-Xyl when rotating the corresponding angles for the Fuc-Gal disaccharide moiety. (*d*) and (*e*) Relevant interproton distances of **2**; Fuc-1-H–Gal-2-H and Fuc-5-H–Xyl-3-H, respectively. The levels are drawn at 2.5, 3.0 and 3.5 Å. (*B*) Trajectory plots for the solvated MD simulation for **2**, starting from minimum A. (*a*) Trajectory of the simulation in Φ/Ψspace for Gal-Xyl. (*b*) History of $\Phi$for Gal-Xyl. (*c*) History of $\Psi$for Gal-Xyl. (*d*) Trajectory of the simulation in Φ/Ψspace for Fuc-Gal. (*e*) History of Φ for Fuc-Gal. (*f*) History of Ψ for Fuc-Gal. (*g*) History of Gal-1-H–Xyl-2-H distance. (*h*) History of Fuc-1-H–Gal-2-H distance. (*i*) History of Fuc-5-H–Xyl-3-H distance.

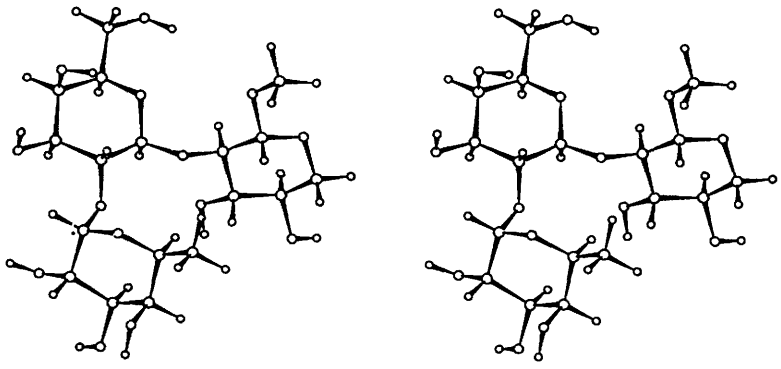

Fig. 4 Stereoscopic view of the MM3* global minimum of 2

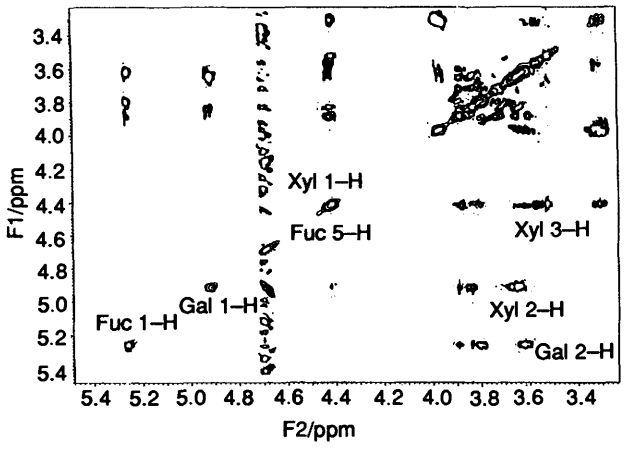

Fig. 5 Relevant inter-residue NOEs for the anomeric protons of 2. 2D-ROESY spectrum, mixing time 300 ms.

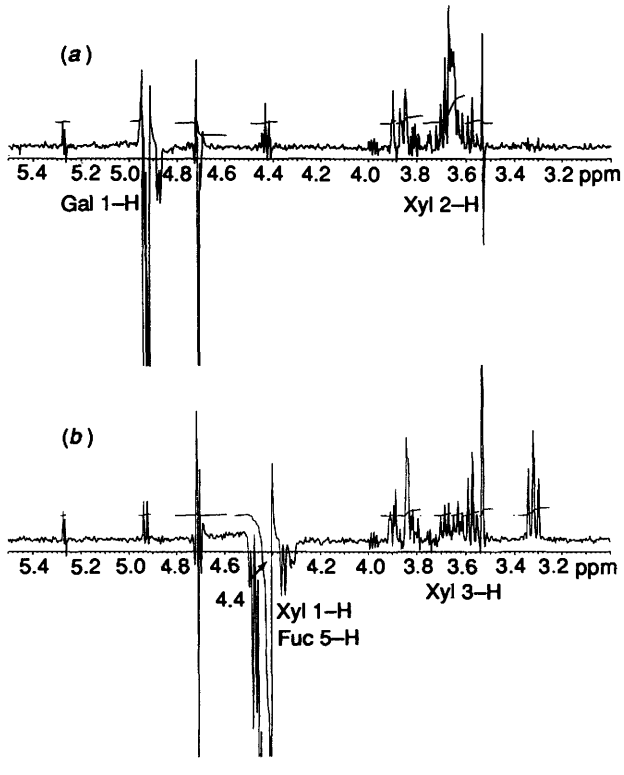

Fig. 6 1D-ROESY experiments (mixing time, 250 ms) for compound 2. (*a*) Selective inversion of the Gal-1-H proton. (*b*) Inversion of the Xyl-1-H and Fuc-5-H protons. Relevant inter-residue NOEs are indicated.

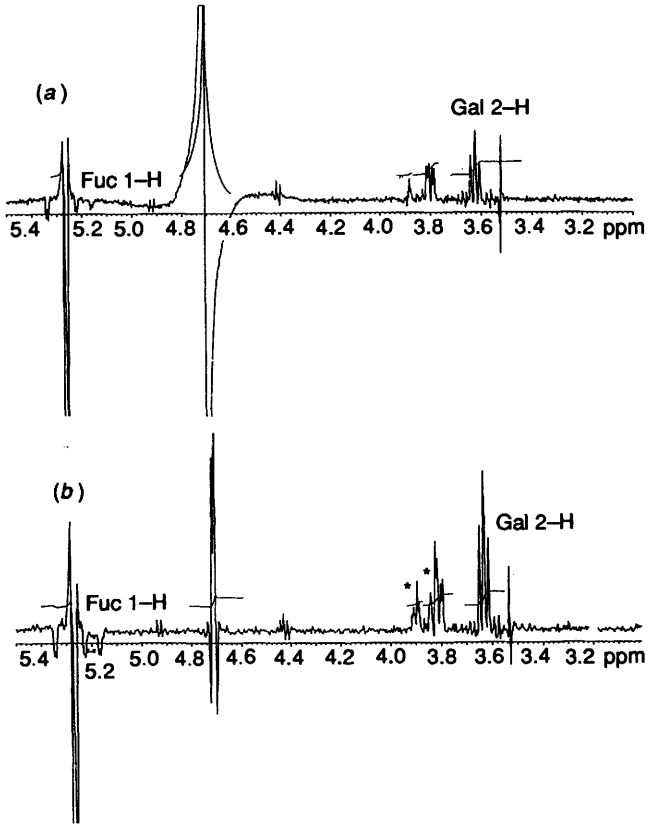

Fig. 7 Comparison of (*a*) 1D-T-ROESY and (*b*) 1D-ROESY spectra taken after selective inversion of the Fuc-1-H proton. The asterisks denote the Hartmann–Hahn contribution which is created during the spin-lock time in the 1D-ROESY spectrum. Relevant inter-residue NOEs are indicated.

maps for **1** and **2**. It is observed that the Gal-1-H–Xyl-2-H distance presents the intersection with the region corresponding to minimum A (A′ for **2**), and therefore, the value of the NOE between these two protons will be sensitive to its population. In an analogous manner, for compound **2**, Fuc-1-H–Gal-2-H and Fuc-5-H–Xyl-3-H NOEs are also representative of the population around minimum A′ and the existence of Fuc-5-H–Gal-2-H NOE will also indicate the contribution of A′ or C′ conformers. Table 6 presents the interproton average $\langle r^{-6}\rangle^{-1/6}$ distances, obtained as indicated in the experimental section, in comparison with the values of interproton distances estimated from the transient experiments.[47] The agreement between experimental and expected results from the population distributions is satisfactory. Note that for **2**, not only the direct inter-residue contacts, Fuc-1-H–Gal-2-H and Gal-1-H–Xyl-2-H, are correctly estimated, but also the remote Fuc-5-H–Xyl-3-H distance is well predicted by the calculations. In addition,

Table 2 Experimental and calculated steady state NOEs (saturation time = 10 s) for **1** at 30 °C in D_2O solution, at 300 and 500 MHz

	Intensity (%)						
Proton pair	*a*	*b*	*c*	*d*	*e*	*f*	*g*
Gal-1-H–Gal-2-H	4.3	6.5	4.8	4.7	2.0	4.7	4.7
Gal-1-H–Gal-3-H	8.7	9.1	5.9	5.7	6.7	5.8	6.4
Gal-1-H–Gal-4-H	−2.1	−3.3	−1.1	−1.1	−1.2	−1.1	−1.2
Gal-1-H–Gal-5-H	10.0	10.5	10.1	9.6	10.6	10.2	9.4
Gal-1-H–Xyl-1-H	<0.5	<0.5	<0.5	14.8	<0.5	<0.5	<0.5
Gal-1-H–Xyl-2-H	12.7	14.0	12.3	0.4	0.2	13.3	14.6
Gal-1-H–Xyl-3-H	<0.5	<0.5	1.1	10.9	0.5	1.5	1.0
Xyl-1-H–Xyl-2-H	1.0	2.5	2.7	3.5	2.0	2.6	2.6
Xyl-1-H–Xyl-3-H	7.6	9.0	7.5	3.0	7.0	7.3	7.5
Xyl-1-H–Xyl-5-H_{ax}	5.8	7.1	5.5	5.4	5.9	5.6	5.5

[a] Experimental 500 MHz. [b] Exp. 300 MHz. [c] Min *a*. [d] Min *b*. [e] Min *c*. [f] MM3*. [g] MD-MM3* (ε = 4). In all calculated cases $\tau_c = 6 \times 10^{-11}$ s and ε = 4 D, 500 MHz.

Table 3 Experimental and calculated steady-state NOEs (saturation time = 10 s) for **2** at 30 °C in D_2O solution at 300 and 500 MHz

	Intensity (%)						
Proton pair	Exp 300 MHz	Exp 500 MHz	H_2O, MD (1 ns)	ε = 80, MD (1 ns)	ε = 1, MD (2 ns)	ε = 4, MD (1 ns)	ε = 4, MM (relaxed)
Fuc-1-H–Fuc-2-H	19.4	15.7	15.7	16.6	16.1	16.6	16.1
Fuc-1-H–Fuc-3-H	2.5	0.8	0.3	0.2	0.3	0.2	0.2
Fuc-1-H–Fuc-5-H	1.0	0.8	0.3	0.4	0.4	0.3	0.3
Fuc-1-H–Gal-2-H	22.5	15.3	15.0	14.7	17.7	14.1	12.3
Fuc-1-H–Gal-3-H	1.3	0.8	0.6	0.8	0.6	0.9	1.1
Gal-1-H–Xyl-2-H	12.4	11.8	11.1	13.6	11.8	12.5	10.4
Gal-1-H–Xyl-3-H	0.8	0.6	0.7	0.2	0.3	0.4	0.6
Gal-1-H–Gal-2-H	20.8*	10.0*	2.4	2.5	2.2	2.6	2.6
Gal-1-H–Gal-3-H	7.6	5.6	5.6	5.2	5.3	5.4	4.9
Gal-1-H–Gal-5-H	20.8*	10.0*	6.8	7.5	6.5	7.4	8.2
Xyl-1-H–Xyl-2-H	3.8	2.4	2.2	2.0	2.1	2.1	2.3
Xyl-1-H–Xyl-3-H	13.1*	11.1*	4.6	5.2	6.1	5.0	4.2
Xyl-1-H–Xyl-5-H_{ax}	6.9	4.0	3.6	3.6	3.5	3.7	3.8
Xyl-1-H–Gal-1-H	1.0	1.4	0.0	0.0	0.3	0.0	0.3
Fuc-5-H–Fuc-3-H	8.0	7.9	7.5	7.8	6.9	7.9	7.0
Fuc-5-H–Fuc-4-H	12.5	9.3	7.9	7.6	8.3	7.5	7.5
Fuc-5-H–Fuc-Me	8.2	7.9	9.0	9.0	9.0	9.0	8.7
Fuc-5-H–Gal-2-H	2.2	2.2	1.0	0.9	0.4	1.1	2.2
Fuc-5-H–Gal-3-H	1.3	2.0	0.1	0.1	0.1	0.0	0.1
Fuc-5-H–Xyl-3-H	13.1*	11.1*	5.9	3.6	2.0	5.3	8.0

[a] Experimental 300 MHz. [b] Exp. 500 MHz. In all calculated cases $\tau_c = 6 \times 10^{-11}$ s and ε = 4 D, 500 MHz. The asterisks denote overlapping signals.

Table 4 Experimental and expected normalized NOESY (mixing 500 ms) and ROESY (mixing 400 ms) intensities (%) for compound **1** in D_2O

	Mixing time/ms					
Proton pair	NOESY[a]	NOESY[b]	NOESY[c]	ROESY[a]	ROESY[b]	ROESY[c]
Gal-1-H–Gal-2-H[a]	0.9	0.9	0.9	0.8	0.8	0.8
Gal-1-H–Gal-3-H	1.9	2.2	2.0	1.6	2.0	1.8
Gal-1-H–Gal-5-H	4.4	3.8	4.0	4.0	3.5	3.7
Gal-1-H–Xyl-2-H	3.9	4.4	3.8	4.1	4.0	3.5
Xyl-1-H–Xyl-2-H	0.7	0.9	0.8	0.6	0.8	0.8
Xyl-1-H–Xyl-3-H	2.2	2.1	2.0	2.1	1.9	1.8
Xyl-1-H–Xyl-5-H_{ax}	2.9	3.3	3.3	2.7	3.1	3.1

[a] Experimental. [b] MD, ε = 4. [c] MM, ε = 4.

we have employed a quantitative approach for our analysis, using a full relaxation matrix [34,48] for the systems under study. Although the model is rather simple, both in the computational calculation and in the NOE derivation (rigid body, isotropic motion), it can be observed that for disaccharide **1**, both the consideration of minimum A or the complete distribution from the relaxed map or the MD simulation provides a satisfactory agreement between the experimental and expected NOEs. For trisaccharide **2**, no single conformer can explain satisfactorily the experimental data and the best match is found when considering the results from the MD simulations (particularly those obtained by the solvated model, although the results obtained in the different simulations are very similar). The observed non-selective relaxation times (Table 5) qualitatively agree (according to their ratio at two different fields) with major flexibility for the external residues (smaller ratios) in compari-

Table 5 Experimental T_1 and calculated T_1 ratios (500/300 MHz) for **2** at 37 °C in D_2O

	Proton											
	1-H		2-H	3-H		5-H_{ax}		5-H_{eq}		6-H_S		6'-H_R
Residue	T_1	Ratio	T_1	T_1	Ratio	T_1	Ratio	T_1	Ratio	T_1	Ratio	T_1
Xyl	0.80,[a] 0.65[b]	1.23	1.19[a]	1.08,[a] 0.85[b]	1.27	0.41,[a] 0.29[b]	1.41	0.48,[a] 0.38[b]	1.26	—	—	—
Gal	0.77,[a] 0.45[b]	1.71	—	—	—	—	—	—	—	0.49,[a] 0.45[b]	1.09	0.57[a]
Fuc	1.04,[a] 0.75[b]	1.38	—	—	—	0.65,[a] 0.61[b]	1.06	—	—	0.55,[a] 0.48[b]	1.14	—

[a] Experimental 500 MHz. [b] Experimental 300 MHz.

Table 6 Calculated average distances[a] (Å) from NOE experiments and molecular mechanics and dynamics[b] calculations for **1** and **2** in D_2O

	Distance/Å						
Proton pair	NOESY (1)	ROESY (1)	NOESY (2)	ROESY (2)	T-ROESY (2)	MD	MM
Fuc-1-H–Fuc-2-H	—	—	2.5	2.5	2.5	2.41	2.44
Fuc-1-H–Gal-1-H	—	—	> 3.5	> 3.5	> 3.5	4.46	4.32
Fuc-1-H–Gal-2-H	—	—	2.3–2.4	2.3–2.4	2.3–2.4	2.33	2.43
Fuc-1-H–Gal-3-H	—	—	> 3.0	> 3.0	> 3.0	3.48	3.35
Gal-1-H–Xyl-1-H	> 3.5	> 3.5	> 3.5	> 3.5	> 3.5	4.44	4.52
Gal-1-H–Xyl-2-H	2.3–2.4	2.3–2.4	2.2–2.3	2.1–2.2	2.2–2.3	2.34	2.45
Gal-1-H–Xyl-3-H	> 3.0	> 3.0	> 3.0	> 3.0	> 3.0	3.78	3.57
Gal-1-H–Gal-3-H	2.55	2.55	2.55	2.55	2.55	2.62	2.67
Xyl-1-H–Xyl-3-H	2.55	2.55	2.55	2.55	2.55	2.68	2.67
Fuc-5-H–Fuc-3-H	—	—	2.5	2.5	2.5	2.57	2.59
Fuc-5-H–Fuc-4-H	—	—	2.5	2.5	2.5	2.44	2.46
Fuc-5-H–Gal-2-H	—	—	> 3.0	> 3.0	> 3.0	3.60	3.22
Fuc-5-H–Xyl-3-H	—	—	2.6–2.9	2.7–2.9	2.6–2.9	2.70	2.41

[a] Intra-residue distances are used for calibration. [b] Distances from MD are the average values of the different simulations.

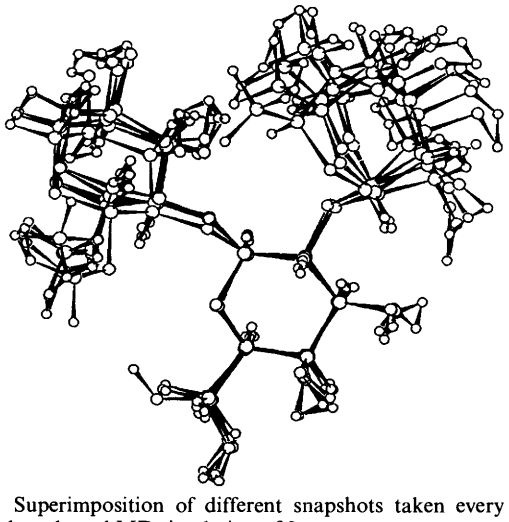

Fig. 8 Superimposition of different snapshots taken every 100 ps during the solvated MD simulation of **2**

son with the internal one.[49] Therefore, for compound **1**, the experimental NOEs can be explained by a population distribution around conformer A with negligible participation of conformers located in islands B or C. For **2**, there is important flexibility for both glycosidic linkages (Fig. 8), around their low energy regions, and *ca.* 15% of both energy surfaces are populated in solution. From the NOE values and the calculations it can be deduced that there is no major change in the conformation of the Gal-Xyl linkage after fucosylation of the galactose residue. According to our results, the glycosidic bonds of **1** are as flexible as those previously reported for Glc-β-(1→2)-Glc (sophorose), on the basis of molecular mechanics calculations and its major conformation is similar to that proposed for cyclic β(1→2)-linked glucans.[50] On the other hand, **2** shows a moderate flexibility around for their glycosidic linkages in the low energy regions, which is similar to those described for similar trisaccharides with the same fucosyl-galactose moiety, but which differ in the third residue. Nevertheless, a more precise evaluation of the population distribution is precluded by the uncertainty in the timescale of motion around the linkages. It can be concluded, according to our results, that the MM3* force field, when used under these conditions (bulk relative permittivity or GB–SA solvent),[28] does satisfactorily reproduce the conformational properties of **1** and **2**. Therefore, this force field may be used within the limits of confidence for conformational analysis of carbohydrate molecules. However, from the NMR experimental point of view, T-ROESY experiments[45] are recommended to eliminate adequately the spurious Hartmann–Hahn contribution[46] in spin-locked NOE experiments of oligosaccharides.

Finally, the conformational entropy at 300 K of each glycosidic linkage associated with the ensemble was estimated to be 2 kcal mol^{-1}. Therefore, according to Carver and co-workers,[7] the freezing of this ligand upon binding to a protein would represent an approximate entropy loss of this magnitude. Besides this associated entropic loss, the molecular recognition of conformers located in regions different to those described above should be accompanied by the formation of hydrogen bonds or by the establishment of stabilizing van der Waals contacts to override the energy barrier between the low energy area and the different islands.[51]

Experimental

Materials

Compounds **1** and **2** were prepared as previously described.[23]

NMR experiments

NMR spectra were recorded at 30 °C in D_2O on Varian XL-300 and Unity 500 spectrometers using a *ca.* 15 mmol dm^{-3} sample, carefully degassed and sealed under argon. Proton chemical

shifts were referenced to residual HDO at δ 4.71 and carbon chemical shifts to external dioxane at δ 67.4.

Selective 1D-TOCSY experiments (mixing time 100 ms) were performed with excitation of the desired anomeric proton with an E-BURP[52] selective pulse.[53]

The 2D rotating frame NOE (ROESY, CAMELSPIN)[44] experiment were recorded at 500 MHz. The total mixing time was set to 150, 300, 400, 450 and 600 ms. The RF carrier was set at δ 6.0 to minimize spurious Hartmann–Hahn effects.[46]

Selective 1D-ROESY experiments were also performed. Spin-locking times of 100, 250, 400 and 550 ms were employed after inversion of the desired proton with a top-hat selective pulse.

Selective 1D-T-ROESY experiments were carried out using the sequence proposed by Hwang and Shaka.[45] Times of 100, 250, 400 and 550 ms were employed for mixing after inversion of the chosen signal with a top-hat selective pulse.[53]

The 2D-NOESY experiments were carried out at 300 and 500 MHz with mixing times of 500, 700, 800 and 1000 ms. NOESY and ROESY were integrated using standard Varian software after applying a third-order polynomial baseline correction in F_2. The total intensity of the added F_1 cross-sections containing diagonal and cross-peaks was given a 100% value.[54] The ROESY intensities were corrected according to their offset.

The steady-state NOEs were obtained at 300 and 500 MHz through the interleaved differential technique using a saturation delay of 10 s. 512 Free induction decays were accumulated for each irradiation site and the experiment was repeated three times at each field. For all the NOE experiments, the intensity of the partially overlapping Xyl-1-H–Xyl-3-H and Fuc-5-H–Xyl-3-H cross-peaks or enhancements were compared with that of Xyl-1-H–Xyl-5-H_{ax}. Since Xyl-3-H is a fixed distance from Xyl-1-H, and, in addition, it is possible to have an exact measurement of the Xyl-1-H–Xyl-5-H_{ax} NOE, the independent contribution of Xyl-1-H–Xyl-3-H was calculated according to a relaxation matrix approach. Fuc-5-H–Xyl-3-H was then estimated from direct subtraction. Since the relevant protons for the NOE calculations are not affected by strong coupling effects, no effort was made to account for these effects.

The pure absorption one bond proton–carbon correlation experiments were collected in the ^{1}H-detection mode using the HSMQC pulse sequence[38] at 500 MHz and a reverse probe. A relaxation delay of 1 s and a delay corresponding to a J value of 150 Hz were used. A BIRD-pulse was used to minimize the signals arising from protons bonded to ^{12}C. ^{13}C-decoupling was not applied in order to estimate the direct proton–carbon couplings.

^{1}H NMR non-selective spin lattice relaxation times[35] were determined at 500 and 300 MHz through the inversion recovery technique using Varian software. Two independent sets of eight delays were used in both determinations.

Conformational calculations

Molecular mechanics. Glycosidic torsion angles are defined as Φ(1′-H–C-1′-O-1′-C-X), and Ψ(C-1′-O-1′-C-X-H-X). Relaxed (Φ,Ψ) potential energy maps were calculated for **1** by using the MM3* force field[20] as integrated in Macromodel.[55] This program differs from the regular MM3 force field in the treatment of the electrostatic terms, since it employs charge–charge instead of dipole–dipole interactions.[56] Only the *gt* conformation was used for the galactose residue.[41] The starting position for the secondary hydroxy groups was set as *r* (anti-clockwise). The previous step involved the generation of the corresponding rigid residue maps by using a grid step of 18°. Then, every Φ,Ψ point of this map was optimized using 100 steepest descent steps, following by 500 conjugate gradient iterations. Following this protocol, the maximum rms derivative in low energy regions was smaller than 0.01 kcal mol^{-1} Å^{-1}.

Molecular dynamics. The geometries describing local minima for **1** and **2** were extensively minimized using conjugate gradients with MM3* (ε = 4) for **1** and (ε = 1, 4 and 80) for **2**, and then taken as starting structures for molecular dynamics simulations *in vacuo* by using the same force field and relative permittivity. The temperature for the simulations was set to 300 K and a time step of 1 fs. Shake[57] was used for the MM3* simulations. The equilibration time was 100 ps, while the total simulation time was 1000 (ε = 80 and 4) or 2000 ps (ε = 1). In addition, an additional 1 ns simulation was performed with the trisaccharide solvated by water, according to the GB–SA model[28] described by Still and co-workers. The temperature was controlled during the equilibration and simulation periods by coupling to a bath,[58] using an exponential decay constant of 0.2 ps. During the equilibration period, the velocities were scaled when the difference between the actual and the required temperature was higher than 10°. Trajectory frames were saved every ps. In all cases, the trajectories were examined with the analysis module of INSIGHT II,[59] or with software written at home.

Probability calculations. From the energy maps calculated for each relative permittivity, the probability distribution was calculated for each Φ,Ψ point, using the Boltzmann equation at 300 K.

The conformational entropy S associated with the ensemble was estimated, according to Carver,[7] as $S = -R\Sigma_i(p_i Ln p_i)$.

NOE calculations. The first step in the NOE calculations was to estimate the interproton average distances, r_{kl}. The previously estimated probability distributions were used to calculate the average distances according to eqn. (1).

$$\langle r^{-6}\rangle_{kl} = \Sigma P_{(\Phi\Psi)} \times r^{-6}_{kl(\Phi\Psi)} \quad (1)$$

The steady-state 1D-NOEs were calculated according to the complete relaxation matrix method by solving the simultaneous set of linear equations proposed by Noggle and Schrimer,[60] and using the average relaxation rates (from $\langle r^{-6}\rangle_{kl}$) calculated from the relaxed relative energies at 300 K using software written at home. The NOEs were also calculated from the MD trajectories. Isotropic motion and external relaxation of 0.1 or 0.2 s were assumed in different calculations. Since NOEs are extremely dependent on the correlation time, different τ_c values were used in order to get the best match between the experimental and the calculated NOE for a given intraresidue proton pair. The best τ_c values were 0.06 ns for **1** and 0.17 ns for **2**. NOESY and ROESY spectra were also simulated for the average distances obtained from the probability distributions or from the MD simulations, using the protocol outlined by Cagas and Bush.[61] The programs used for simulating 1D-NOE, NOESY and/or ROESY experiments for the ensemble average distribution of conformers or from MD simulations are available from the authors. Interproton distances were also estimated from the experimental NOESY, ROESY and T-ROESY experiments making use of the isolated spin approximation,[47] by extrapolation of the build-up curves at the mixing time, $\tau_m = 0$.

Acknowledgements

Financial support by DGICYT (grant PB87-0367) is gratefully acknowledged. M. M. P., J. L. A. and R. L. thank Europharma S.A. for fellowships. We thank Professor Martín-Lomas and Dr Fernández-Mayoralas for their interest and support throughout this work.

References

1 M. L. Phillips, E. Nudelman, F. C. A. Gaeta, M. Perez, A. K. Shingai, S. Hakomori and J. C. Paulson, *Science*, 1990, **250**, 1130.

2 J. M. Harlan and D. Y. Liu, *Adhesion: Its Role in Inflammatory Disease*, Freeman, New York, 1992, pp. 19–64.
3 (*a*) K. G. Rice, P. Wu, L. Brand and Y. C. Lee, *Curr. Opin. Struct. Biol.*, 1993, **3**, 669; (*b*) C. A. Bush, *Curr. Opin. Struc. Biol.*, 1992, **2**, 655.
4 Y. Bourne, H. van Tielbeurgh and C. Cambillau, *Curr. Opin. Struc. Biol.*, 1993, **3**, 681.
5 M. Hricovini, R. N. Shah and J. P. Carver, *Biochemistry*, 1992, **31**, 10018.
6 (*a*) R. U. Lemieux, K. Bock, L. T. J. Delbaere, S. Koto and V. S. Rao, *Can. J. Chem.*, 1980, **58**, 631; (*b*) R. U. Lemieux, *Chem. Soc. Rev.*, 1989, **18**, 347; (*c*) R. U. Lemieux, L. T. J. Delbaere, H. Beierbeck and U. Spohr, in *Host–guest molecular interactions: from chemistry to biology*, CIBA Foundation Symp. 158, Wiley, Chichester, 1991, 231.
7 (*a*) D. A. Cumming and J. P. Carver, *Biochemistry*, 1987, **26**, 6664; (*b*) J. P. Carver, S. W. Michnick, A. Imberty and D. A. Cumming, in *Carbohydrate Recognition in Cellular Function*, CIBA Foundation Symp. 145, Wiley, Chichester, 1989, 6; (*c*) J. P. Carver, *Pure Appl. Chem.*, 1993, **65**, 763.
8 M. S. Searle and D. H. Williams, *J. Am. Chem. Soc.*, 1992, **114**, 10690.
9 J. A. McCammon and S. C. Harvey, *Dynamics of Proteins and Nucleic Acids*, Cambridge University Press, Cambridge, 1987.
10 (*a*) J. W. Brady and R. K. Schmidt, *J. Phys. Chem.*, 1993, **97**, 958, and refs. therein; (*b*) *Computer Modelling of Carbohydrate Molecules*, eds. A. D. French and J. W. Brady, ACS Symposium Series 430, Am. Chem. Soc., Washington DC, 1990.
11 B. J. Hardy and A. Sarko, *J. Comput. Chem.*, 1993, **7**, 831.
12 P. D. J. Grootenhuis and C. A. G. Haasnoot, *Molecular Simulation*, 1993, **10**, 75.
13 M. K. Dowd, J. Zeng, A. D. French and P. J. Reilly, *Carbohydr. Res.*, 1992, **230**, 223.
14 S. Engelsen and K. Rasmussen, *Int. J. Biol. Macromol.*, 1993, **15**, 56.
15 A. J. Duben, M. Hricovini and I. Tvaroska, *Carbohydr. Res.*, 1993, **247**, 71.
16 B. R. Leeflang, J. F. G. Vliegenthart, L. M. J. Kroon-Batenburg, B. P. van Eijck and J. Kroon, *Carbohydr. Res.*, 1992, **230**, 41.
17 J. N. Scarsdale, J. H. Prestegard and R. K. Yu, *Biochemistry*, 1990, **29**, 9843.
18 A. Imberty, K. D. Hardman, J. P. Carver and S. Perez, *Glycobiology*, 1991, **1**, 456.
19 S. W. Homans, *Biochemistry*, 1990, **29**, 9110.
20 N. L. Allinger, Y. H. Yuh and J.-H. Lii, *J. Am. Chem. Soc.*, 1989, **111**, 8551.
21 (*a*) A. Rivera-Sagredo, D. Solís, T. Díaz-Mauriño, J. Jiménez-Barbero and M. Martín-Lomas, *Eur. J. Biochem.*, 1991, **197**, 217; (*b*) D. Solís, P. Fernandez, T. Díaz-Mauriño, J. Jiménez-Barbero and M. Martín-Lomas, *Eur. J. Biochem.*, 1993, **214**, 677 and refs. therein.
22 (*a*) M. Bernabé, A. Fernández-Mayoralas, J. Jiménez-Barbero, M. Martín-Lomas and A. Rivera, *J. Chem. Soc., Perkin Trans. 2*, 1989, 1867; (*b*) A. Rivera-Sagredo, F. J. Cañada, O. Nieto, J. Jiménez-Barbero and M. Martín-Lomas, *Eur. J. Biochem.*, 1992, **209**, 415; (*c*) D. Solís, J. Jiménez-Barbero, M. Martín-Lomas and T. Diaz-Mauriño, *Eur. J. Biochem.*, 1994, **223**, 107.
23 R. Lopez, E. Montero, F. Sanchez, F. J. Cañada and A. Fernández-Mayoralas, *J. Org. Chem.*, 1994, **59**, 7027.
24 W. S. York, A. G. Darvill and P. Albersheim, *Plant Physiol.*, 1984, **75**, 295.
25 P. Albersheim, A. G. Darvill, C. Augur, J. J. Cheong, S. S. Eberhard, M. G. Hahn, V. Marfa, D. Mohnen, M. A. O'Neill, M. D. Spiro and W. S. York, *Acc. Chem. Res.*, 1992, **25**, 77.
26 (*a*) M. K. Dowd, A. D. French and P. J. Reilly, *Carbohydr. Res.*, 1992, **233**, 15; (*b*) A. D. French and M. K. Dowd, *J. Mol. Struct. (Theochem.)*, 1993, **286**, 183.
27 R. U. Lemieux, K. Bock, L. T. J. Delbaere, S. Koto and V. S. R. Rao, *Can. J. Chem.*, 1980, **58**, 631.
28 W. C. Still, A. Tempczyk, R. C. Hawley and T. Hendrickson, *J. Am. Chem. Soc.*, 1990, **112**, 6127.
29 C. A. Bush and P. Cagas, *Adv. Biophys. Chem.*, 1992, **2**, 149.
30 L. Toma, P. Ciuffreda, D. Colombo, F. Ronchetti, L. Lay and L. Panza, *Helv. Chim. Acta*, 1994, **77**, 668.
31 C. Mukhopadhyay and C. A. Bush, *Biopolymers*, 1991, **31**, 1737, and refs. therein.
32 G. Widmalm and R. M. Venable, *Biopolymers*, 1994, **34**, 1079.
33 A. Ejchart, J. Dabrowski and C. W. von der Lieth, *Magn. Reson. Chem.*, 1992, **30**, S105.
34 D. Neuhaus and M. P. Williamson, *The Nuclear Overhauser Effect in Structural and Conformational Analysis*, VCH Publishers, New York, 1989.
35 P. Dais and A. S. Perlin, *Adv. Carbohydr. Chem. Biochem.*, 1987, **45**, 125.
36 U. Piantini, O. W. Sorensen and R. R. Ernst, *J. Am. Chem. Soc.*, 1982, **104**, 6800.
37 A. Bax and D. G. Davis, *J. Magn. Reson.*, 1988, **63**, 355.
38 E. R. P. Zuiderweg, *J. Magn. Reson.*, 1990, **67**, 565.
39 Y. Nishida, H. Hori, H. Ohrui and H. Meguro, *J. Carbohydr. Chem.*, 1988, **7**, 239.
40 Y. Nishida, H. Ohrui and H. Meguro, *Tetrahedron Lett.*, 1984, **25**, 1575.
41 (*a*) L. M. J. Kroon-Batenburg and J. Kroon, *Biopolymers*, 1990, **29**, 1243; (*b*) W. M. Mackie, A. Maradufu and A. S. Perlin, *Carbohydr. Res.*, 1986, **150**, 23.
42 K. Bock and S. Refn, *Acta Chem. Scand. B*, 1987, **41**, 469.
43 A. Kumar, R. R. Ernst and K. Wüthrich, *Biochem. Biophys. Res. Comm.*, 1980, **95**, 1.
44 A. A. Bothner-By, R. L. Stephens, J.-M. Lee, C. D. Warren and R. W. Jeanloz, *J. Am. Chem. Soc.*, 1984, **106**, 811.
45 T. L. Hwang and A. J. Shaka, *J. Am. Chem. Soc.*, 1992, **114**, 3157.
46 A. Bax and D. G. Davis, *J. Magn. Reson.*, 1985, **63**, 207.
47 S. Macura and R. R. Ernst, *Mol. Phys.*, 1980, **41**, 95.
48 (*a*) T. Peters, J. R. Brisson and D. R. Bundle, *Can. J. Chem.*, 1990, **68**, 979; (*b*) A. Imberty, V. Tran and S. Perez, *J. Comput. Chem.*, 1989, **11**, 205.
49 H. van Halbeek and L. Poppe, *Magn. Reson. Chem.*, 1992, **30**, S74.
50 W. S. York, J. U. Thomsen and B. Meyer, *Carbohydr. Res.*, 1993, **248**, 55.
51 A. Imberty, Y. Bourne, C. Cambillau, P. Rouge and S. Perez, *Adv. Biophys. Chem.*, 1993, **3**, 71.
52 H. Geen and R. Freeman, *J. Magn. Reson.*, 1991, **93**, 93.
53 R. Freeman, *Chem. Rev.*, 1991, **91**, 1397.
54 J. Breg, L. M. J. Kroon-Batenburg, G. Strecker, J. Montreuil and J. F. G. Vliegenthart, *Eur. J. Biochem.*, 1989, **178**, 727.
55 F. Mohamadi, N. G. J. Richards, W. C. Guida, R. Liskamp, C. Caufield, G. Chang, T. Hendrickson and W. C. Still, Macromodel V3.5x, *J. Comput. Chem.*, 1990, **11**, 440.
56 N. L. Allinger and U. Burkert, *Molecular Mechanics*, Am. Chem. Soc., Washington DC, 1982.
57 W. F. van Gunsteren and H. J. C. Berendsen, *Mol. Phys.*, 1977, **34**, 1311.
58 H. J. C. Berendsen, J. P. M. Postma, W. F. van Gunsteren, A. Di Nola and J. R. Haak, *J. Chem. Phys.*, 1984, **81**, 3684.
59 Insight II 2.1.0, Program, Biosym Technol. Inc., San Diego, USA.
60 J. H. Noggle and R. E. Schirmer, *The Nuclear Overhauser Effect: Chemical Applications*, Academic Press, New York, 1971, pp. 90–93.
61 P. Cagas and C. A. Bush, *Biopolymers*, 1990, **30**, 1123.

Paper 4/06813K
Received 8*th November* 1994
Accepted 29*th November* 1994